Assessment of fluctuating velocities in disturbed cardiovascular blood flow: in vivo feasibility of generalized phase-contrast MRI

Petter Dyverfeldt, John-Peder Escobar Kvitting, Andreas Sigfridsson, Jan Engvall, Ann F Bolger and Tino Ebbers

This is the pre-reviewed version of the following article:

Petter Dyverfeldt, John-Peder Escobar Kvitting, Andreas Sigfridsson, Jan Engvall, Ann F Bolger and Tino Ebbers, Assessment of fluctuating velocities in disturbed cardiovascular blood flow: in vivo feasibility of generalized phase-contrast MRI, 2008, Journal of Magnetic Resonance Imaging, (28), 3, 655-663.

which has been published in final form at:
http://dx.doi.org/10.1002/jmri.21475

Assessment of Fluctuating Velocities in Disturbed Cardiovascular Blood Flow: In-Vivo Feasibility of Generalized Phase-Contrast MRI

Petter Dyverfeldt (MS) [1,2,3], John-Peder Escobar Kvitting (MD, PhD) [1,3], Andreas Sigfridsson (MS) [1,3,4], Jan Engvall (MD, PhD) [1,3], Ann F. Bolger (MD) [1,5], Tino Ebbers (PhD)[1,3]

[1] Division of Cardiovascular Medicine, Department of Medical and Health Sciences, Linköping University, Linköping, Sweden.

[2] Division of Applied Thermodynamics and Fluid Mechanics, Department of Management and Engineering, Linköping University, Linköping, Sweden.

[3] Center for Medical Image Science and Visualization (CMIV), Linköping University, Linköping, Sweden.

[4] Division of Medical Informatics, Department of Biomedical Engineering, Linköping University, Linköping, Sweden.

[5] Department of Medicine, University of California San Francisco, San Francisco, California, United States.

Correspondence: Petter Dyverfeldt, MS, Division of Cardiovascular Medicine,
Department of Medical and Health Sciences, Linköping University,
SE-581 85 Linköping, Sweden.
E-mail: petter.dyverfeldt@cmiv.liu.se

Grant support: Swedish Research Council, The Swedish Heart-Lung Foundation

Running Title: Generalized PC-MRI in Disturbed Blood Flow

Word count: 4998

ABSTRACT

Purpose: To evaluate the feasibility of generalized phase-contrast magnetic resonance imaging (PC-MRI) for the non-invasive assessment of fluctuating velocities in cardiovascular blood flow.

Materials and Methods: Multidimensional PC-MRI was used in a generalized manner to map mean flow velocities and intravoxel velocity standard deviation (IVSD) values in one healthy aorta and in three patients with different cardiovascular diseases. The acquired data were used to assess the kinetic energy of both the mean (MKE) and the fluctuating (TKE) velocity field.

Results: In all the subjects, both mean and fluctuating flow data were successfully acquired. The highest TKE values in the patients were found at sites characterized by abnormal flow conditions. No regional increase in TKE was found in the normal aorta.

Conclusion: PC-MRI IVSD mapping is able to detect flow abnormalities in a variety of human cardiovascular conditions and shows promise for the quantitative assessment of turbulence. This approach may assist in clarifying the role of disturbed hemodynamics in cardiovascular diseases.

Key Words: Turbulent flow, cardiovascular disease, phase-contrast magnetic resonance imaging, stenosis, intravoxel velocity standard deviation mapping, turbulence.

INTRODUCTION

In cardiovascular medicine, the assessment of blood flow is fundamental to the understanding and detection of disease, and many medical, interventional and surgical treatments may impact the optimization of flow (1).

In the normal arterial tree, fluid transport is maintained with high efficiency and laminar flow is prevalent. The efficiency of fluid transport increases with higher laminar flow rates, and therefore the flow downstream from complex geometries such as heart valves, sharp bends and bifurcations can be suspected to be close to the threshold for the onset of turbulence. Turbulent fluid motion has been described by Hinze (2) as "*an irregular condition of flow in which the various quantities show a random variation with time and space coordinates, so that statistically distinct average values can be discerned*".

Non-laminar flow accompanies many forms of cardiovascular disease (3) where flow obstructions such as valve stenoses or atherosclerotic plaques can introduce flow velocity fluctuations and thereby decrease the transport efficiency of the fluid. In flow containing velocity fluctuations, endothelial cells and blood constituents are exposed to abnormal stresses and are subjected to the risk of hemolysis (4) as well as platelet activation and thrombus formation (5,6). Additionally, ample evidence supports the theory that fluctuating velocities constitute a central factor in the pathogenesis of atherosclerotic plaques at predilection areas such as sharp bends and bifurcations in the vascular tree (3,7,8).

Turbulent blood flow has previously been studied in humans using catheter-based hot-film anemometry (9) and perivascular Doppler ultrasound during open chest situations (10). Non-invasive ultrasound techniques can be applied to the heart and arterial tree at those sites where adequate acoustic windows exist, allowing study of flow behavior in various cardiovascular diseases. Valvular stenoses, for example, are often assessed based on a Doppler measurement of the peak velocity. In principle, Doppler ultrasound methods are able to measure regional velocity distributions and should therefore have the ability to quantify turbulence. A non-invasive method using Doppler echocardiography to study turbulence has been outlined by Izaaz and colleagues (11). However, non-invasive Doppler methods are limited by definition to the assessment of

turbulence only in the single direction defined by the ultrasound beam. The results from such an approach are dependent on the measurement direction and thus limited by assumptions about local flow structures (12).

Magnetic resonance imaging (MRI) offers the unique opportunity to non-invasively acquire multidirectional hemodynamic information anywhere in the human body. The most common MRI method for flow quantification is phase-contrast (PC) MRI velocity mapping (13) which can be used to assess the time-varying three-dimensional cardiovascular blood flow (14). This method exploits the phenomenon that the phase difference between two complex-valued PC-MRI signals acquired with different flow sensitivity will be proportional to the fluid flow velocity. Based on the velocity mapping technique, several aspects of diseased cardiovascular flow can be assessed (15,16). Due to spatial averaging over the voxel, the conventional PC-MRI velocity mapping method measures a sample mean of intravoxel spin velocities. To address this limitation, several methods have exploited the ability of Fourier velocity encoding MRI (13) to obtain an intravoxel velocity resolution and thereby capture the peak velocities (17-19). Nayak et al (19), for example, developed a rapid technique with spiral readout to measure peak velocities in flow jets accompanying valvular stenoses.

Multiple spin velocities within an imaging voxel reduce the magnitude of the complex-valued PC-MRI signal during the influence of a magnetic field gradient (20) and several studies have attempted to establish a relationship between the degree of signal loss and the hemodynamic significance of stenoses (21,22). Oshinski and colleagues (20) showed that turbulent velocity fluctuations are the major cause of signal loss. By considering turbulent velocity fluctuations to give rise to a Gaussian distribution of spin velocities within a voxel, Dyverfeldt et al (23) presented a method to quantify the intravoxel velocity standard deviation (IVSD) in turbulent flow from the magnitude relationship of two PC-MRI signals. This study included a theoretical derivation and an in-vitro validation of the IVSD method but did not comprise in-vivo IVSD examinations.

In this study, the PC-MRI IVSD method is applied in-vivo with the objective of evaluating the feasibility of this method for non-invasive assessment of flow velocity fluctuations in the

pulsatile blood flow of humans. Also, an approach to utilizing this generalization of PC-MRI for direct comparison of the energy content of the mean and the fluctuating velocity field is proposed.

MATERIALS AND METHODS

PC-MRI IVSD Mapping

In addition to mean velocity assessment by conventional velocity mapping, generalized PC-MRI allows for quantitative assessment of turbulent velocity fluctuations by IVSD mapping. The IVSD method, which is described in detail elsewhere (23), is based on the analytical expression describing the complex-valued PC-MRI signal of a voxel in presence of a first gradient moment, M_1 (24):

$$S(k_v) = C\int_{-\infty}^{\infty} s(v)e^{-ik_v v}\mathrm{d}v, \qquad [1]$$

where C is a constant influenced by relaxation parameters, spin density and receiver gain, v is the velocity, $s(v)$ is the spin velocity distribution within the voxel and $k_v = \gamma M_1$. By considering the spin velocities within a voxel to be normally distributed in turbulent flow, $s(v)$ can be expressed as the Gaussian probability density function. Doing this, Eq. 1 can be written as

$$S(k_v) = C\exp\left(-\frac{\sigma^2 k_v^2}{2} - iv_{\mathrm{m}}k_v\right), \qquad [2]$$

where σ [m s^{-1}] is the IVSD. By combining two PC-MRI signals acquired with different first gradient moment, $S(k_{v_1})$ and $S(k_{v_2})$, the IVSD can be obtained from the signal magnitude relationship according to

$$\sigma = sqrt\left[\frac{2}{k_{v_1}^2 - k_{v_2}^2}\ln\left(\left|S(k_{v_2})\right|/\left|S(k_{v_1})\right|\right)\right],\ \left|k_{v_1}\right| \neq \left|k_{v_2}\right|. \qquad [3]$$

Thus, mapping the IVSD requires no data other than what is normally acquired in a standard PC-MRI measurement. A one-directional PC-MRI measurement gives rise to two complex-valued PC-MRI signals, acquired with different flow sensitivity. In velocity mapping, the mean fluid velocity is computed by phase subtraction; in IVSD mapping, in contrast, the IVSD is obtained from the signal magnitude relationship described in Eq. 3 (Fig. 1).

The accuracy of the IVSD method, in the presence of noise, is maximized by acquiring a reference flow encoding segment with zero first gradient moment, $S(0)$ (23). This choice of flow encoding scheme also leads to a direct relationship between k_v in the flow sensitized flow encoding segment, $S(k_v)$, and the velocity encoding range (VENC) according to VENC = π / k_v. In velocity mapping, where velocities outside the VENC are aliased, the VENC defines a strict dynamic range. As phase wraps have no effect on the signal magnitude, the dynamic range in IVSD mapping is not strictly limited by the choice of VENC. Instead, the VENC is related to the IVSD sensitivity. Best sensitivity is achieved at $\tilde{\sigma}$ = VENC/π (23). This corresponds to a signal magnitude ratio $|S(k_v)|/|S(0)|$ of $e^{-1/2}$ which is approximately 0.6.

Assessment of the Kinetic Energy of the Mean and the Fluctuating Velocity Field

By using a bipolar gradient flow encoding scheme consisting of a reference flow encoding segment and a differentially encoded segment in each direction, generalized PC-MRI offers reconstruction of both the mean velocity vector field and the IVSD in three directions. This allows for straightforward analyses of the energy content of the mean and the fluctuating velocity field. Using Reynolds decomposition, a velocity vector field, **U**, can be statistically separated into two components according to

$$\mathbf{U} = \overline{\mathbf{U}} + \mathbf{u} \text{ [m s}^{-1}\text{]}, \quad [4]$$

where $\overline{\mathbf{U}}$ is the mean velocity field, averaged over either time, space or an ensemble, and $\mathbf{u}$ is the fluctuating velocity field which by definition has a mean value of zero (25). While the mean velocity field describes the average flow behavior, small scale changes of the flow are contained within the fluctuating velocity which reflects the irregularity and randomness of turbulence. The root-mean-square of the fluctuating velocity in each direction, i, coincides with the measured IVSD, σ_i, according to

$$\left(\overline{u_i^2}\right)^{1/2} = \sigma_i \text{ [m s}^{-1}\text{]}. \quad [5]$$

The standard deviation squared, multiplied by the fluid density, ρ, yields the Reynolds normal stress, which is the stress acting normal to a fluid element. In the Reynolds, or turbulence, stress tensor, a second-order symmetrical tensor defined as $\rho\overline{u_i u_j}$ [N m^{-2}] with i and j denoting directions, the diagonal elements are the Reynolds normal stresses in three directions. The Reynolds normal stresses add up to the tensor trace, which is an invariant of the Reynolds stress

tensor and thereby insensitive to measurement directions. This tensor trace appears in the expression describing the average kinetic energy per volume unit (K),

$$K = \frac{1}{2}\rho\sum_{i=1}^{3}\overline{U_i}^2 + \frac{1}{2}\rho\sum_{i=1}^{3}\overline{u_i^2} \text{ [J m}^{-3}\text{]}, \quad [6]$$

as a part of the second term on the right hand side which describes the kinetic energy of the fluctuating velocity field (turbulent kinetic energy, TKE). The TKE, which is computed from the IVSD in three directions, is a direction-independent measure of the intensity of turbulence. The first term on the right hand side is the kinetic energy of the mean velocity field (mean kinetic energy, MKE).

Study Population

The in-vivo feasibility of PC-MRI IVSD mapping was evaluated in a range of cardiovascular conditions by imaging a 29-year-old healthy male volunteer and three patients. The first patient was an 80-year-old male with mild aortic valve insufficiency demonstrated on echocardiography; left ventricular flow was examined. The second patient was a 71-year-old male who was 14 months status post implantation of a stented biological aortic valve (Carpentier-Edwards PERIMOUNT, 25 mm diameter); flow was studied downstream from the normally functioning valve prosthesis. The third patient was a 60-year-old female 46 years status post aortic coarctation repair with end-to-end anastomosis that had signs of restenosis in the anastomotic area distal to the left subclavian artery. In addition, in this patient echocardiography also demonstrated an abnormal, minimally obstructive membrane in the left ventricular outflow tract below the aortic valve. Post-stenotic flow in the descending thoracic aorta was studied.

The study was approved by the regional ethics committee for human research at the medical faculty of Linköping University. Written informed consent was obtained from all participants.

Data Acquisition

All measurements were carried out using a clinical 1.5 T scanner (Philips Achieva, Philips Medical Systems, Best, the Netherlands) equipped with high-performance gradients (amplitude 33 mT/m, slew rate 160 T/m/s). Time-resolved three-dimensional (3D) PC-MRI data were acquired during free breathing using a flow compensated gradient echo pulse sequence with interleaved three-directional flow encoding and retrospective, vectorcardiogram controlled, cardiac gating. The bipolar gradient flow encoding scheme included a reference flow encoding

segment and a differentially encoded segment in each direction. Trade-offs between temporal resolution and scan time were enabled by interleaving a multiple of N sets of the four flow encoding segments. To suppress respiratory effects, a navigator gating method (Philips Medical Systems, Best, the Netherlands) using a slowly adapting window position was applied. The navigator monitored the position of the diaphragm during the scanning and imaging data were only accepted at end expiration. All subjects were in sinus rhythm; the effects of variations in cardiac frequency, such as arrhythmias, were minimized by rejecting RR-intervals shorter than 90 % or longer than 120 % of the average duration of the eight preceding RR-intervals.

In three of four examinations, both the IVSD and the velocity were reconstructed from a single acquisition. In the coarctation patient only, separate scans with different VENC settings were used to acquire the velocity and the IVSD data. Knowing that a 40 % signal loss provides the best sensitivity, the VENC settings used in the IVSD measurements in the patients were chosen to provide good accuracy at the highest expected IVSD values. For comparison, the IVSD scan in the healthy volunteer had the same VENC as in the coarctation patient. Parallel imaging by sensitivity encoding (SENSE) with a speed up factor of two was applied in the velocity scan in the coarctation patient and in the single scans in the other two patients (Table 1). A flip angle of 8° was used in all measurements; additional imaging parameters are summarized in Table 1. Anatomical orientation in the patient with aortic valve insufficiency was obtained by standard balanced steady state free precession (b-SSFP) cine imaging. For anatomical orientation in the coarctation patient, a 3D contrast enhanced MRA (field-of-view 360 x 360 x 80 mm, matrix 480 x 480 x 40) was acquired using a Gadolinium contrast agent (Magnevist, Schering, Germany, dose of 0.4 ml/kg) prior to the PC-MRI measurements.

Post Processing and Visualization

On the scanner, all velocity data were corrected for concomitant gradient field effects. A temporal sliding window reconstruction (Philips Medical Systems, Best, The Netherlands) with individual non-linear stretching of each RR-interval, taking into account that the duration of systole is almost constant, was used to reconstruct the time-resolved PC-MRI data into 40 time frames. Using automated post processing, the velocity data were corrected for background errors and phase wraps (26). The TKE and MKE were computed from the IVSD and the velocity data, respectively, according to Eq. 6. In the computations of data along the sample lines in the healthy

volunteer and the coarctation patient, trilinear interpolation was used to extract the values along the sample lines.

The post processed time-resolved 3D data were converted into a file format compatible with commercially available visualization software (EnSight, CEI Inc., Research Triangle Park, NC, USA). This enabled the use of several visualization tools. Iso-surface rendering was used for anatomical delineations. 2D planes and surfaces were extracted from the 3D data volumes and color coded according to scales of TKE in order to visualize the fluctuating velocity fields. Three-dimensional streamlines, color-coded according to scales of speed, were generated in order to visualize the instantaneous 3D velocity fields.

RESULTS

All data were acquired successfully.

Aortic flow at peak systole in the healthy volunteer is shown in Fig. 2. Three dimensional streamlines (Fig. 2a) show no regional increase in velocity. A semicylinder-shaped clip surface color coded according to TKE, combined with a semi-transparent 3D iso-surface rendering computed from the PC-MRI data, shows no regional increase in TKE (Fig. 2b).

The peak regurgitation flow in the patient with mild aortic valve insufficiency is visualized in Fig. 3, along with a semi-transparent b-SSFP three-chamber image. 3D streamlines (Fig. 3a) reveal a small regurgitant flow into the left ventricular outflow tract during diastole, and a 2D TKE clip plane (Fig. 3b) shows elevated values of TKE in connection with the regurgitant jet. The highest TKE values in this region reached 320 J/m^3. The maximum speed was about 1 m/s, which corresponds to an MKE of 530 J/m^3. The streamlines in Fig. 3a were defined from a rectangular grid. Note that, due to myocardial motion and the presence of other lumen regions, non-zero velocities may be observed also outside of the intracardiac flow region.

Visualizations of aortic peak flow in the patient with an aortic valve prosthesis are shown in Fig. 4. The 3D streamlines in Fig. 4a show high speed flow immediately downstream from the valve and complex flow patterns in the ascending aorta. The TKE map in Fig. 4b, combined with a 3D iso-surface rendering of the PC-MRI data, shows that the highest values of TKE are present

downstream from the valve. Elevated values of TKE can also be observed at the outer wall of the ascending aorta. Downstream from the valve, the overall high values of TKE were about 700 J/m^3. The peak flow speed was about 3 m/s, which corresponds to an MKE of 4770 J/m^3.

Figure 5 shows the three different types of data acquired in the coarctation patient. The 3D iso-surface rendering of the contrast-enhanced MRA data in Fig. 5a shows a constriction at the site of the end-to-end aortic anastomosis (arrow). The 3D streamline visualization of the aortic blood flow at peak systole in Fig. 5b reveals a flow jet distal to that stenosis. In Fig. 5c, a convex surface, color-coded according to TKE, is shown with a semi-transparent 3D iso-surface rendering of the contrast-enhanced MRA data. The TKE map demonstrates the energy content of the turbulent velocity fluctuations; the highest values of TKE are observed downstream from the flow jet. In addition, elevated values of TKE are seen in the aortic root downstream from the abnormal subvalvular membrane. A time-resolved visualization of the TKE can be seen in Movie 1. The black line seen in Fig. 5a, originating approximately 3 mm upstream from the aortic re-coarctation, was aligned along the peak systolic velocities of the flow jet seen in Fig. 5b. This line serves as a sample line for data extraction. For comparison, a corresponding sample line, originating distal to the left subclavian artery, was placed in the healthy volunteer. Values of the TKE and MKE along these sample lines over time are shown in Figs. 6 and 7. The maximum TKE and MKE values observed in the coarctation patient were about eight and six times greater than in the healthy volunteer, respectively. In the coarctation patient, the peak TKE value along the sample line was 780 J/m^3. The peak flow speed was 2.8 m/s, which corresponds to an MKE of 4220 J/m^3. A more detailed analysis of the temporal alterations of the kinetic energy components in the coarctation patient can be seen in Fig. 8 where the TKE and MKE are plotted over the cardiac cycle at three different locations. These locations, as indicated by the circles on the sample line in Fig. 5a, correspond to distances approximately one, two and three times the diameter of the stenosis relative to the center of the constriction. Corresponding plots for the healthy volunteer are shown in Fig. 9.

DISCUSSION

It has recently been shown in-vitro that PC-MRI can be used in a generalized manner to quantify IVSD and turbulence intensity (23). In the present study we have extended the generalized PC-MRI approach to in-vivo usage, allowing the assessment of the kinetic energy of both the mean

(MKE) and the fluctuating (TKE) velocity field in human cardiovascular flow. Measurements were made across a spectrum of in-vivo conditions. In all the patients included in this study, sites characterized by abnormal flow behavior distinguished themselves by demonstrating considerably elevated TKE values (Figs. 3-5). The majority of the elevated TKE values can be related to turbulent flow. No regional increase in TKE was found in the healthy volunteer (Fig. 2).

The 3D streamline visualization of the aortic peak flow in the healthy volunteer (Fig. 2a) shows non-complex flow and no regional increase in velocity. Well-organized normal aortic blood flow should not be perturbed by small scale velocity variations in the same order of magnitude as in diseased aortic geometries and the MKE along a sample line comparable to the one in Fig. 5 should be nearly constant in space and only vary temporally due to the cardiac cycle. This is confirmed by the results in Figs. 7 and 9 where the MKE in the healthy volunteer is nearly constant along the sample line for a given time frame and the TKE overall is low. Sites known to contain vortical flow, such as the sinuses of Valsalva (27), either did not result in elevated TKE values. Note, however, that this study was not intended to describe the possible extent of turbulence in normal cardiovascular blood flow. The healthy volunteer was included to demonstrate the differences between normal and pathological flow detected by this approach when using the same measurement settings. An investigation of IVSD values in normal conditions would benefit from a lower VENC value than the one used in the present study.

The diastolic 3D streamlines (Fig. 3a) in the patient with mild aortic valve insufficiency reveal a small regurgitant jet in the left ventricular outflow tract. Elevated TKE values accompany the jet (Fig. 3d). The aortic valve insufficiency did not cause elevated values of TKE at other intraventricular locations. Both the peak values and the spatial distribution of the TKE map may provide a method of assessing the degree of valvular insufficiencies beyond the more semi-quantitative methods currently used. Further studies are needed to assess the relationship between the severity of valvular insufficiency and quantities obtained by IVSD mapping.

In agreement with previous studies of bioprosthetic valve hemodynamics (28,29), IVSD mapping revealed elevated values of TKE downstream from the implanted aortic valve

prosthesis (Fig. 4b). PC-MRI has previously shown great potential for studying flow around prosthetic heart valves in-vivo (30). The additional information obtained by IVSD mapping could be used to assess the impact of valve parameters such as orientation, size and design on the flow after implantation. The ability to link in-vivo valve hemodynamics with parameters such as regression of left ventricular hypertrophy after aortic valve replacement could be of great clinical interest.

Visualization of the peak systolic 3D velocity field in the patient with an aortic coarctation (Fig. 5b) demonstrates a flow jet characterized by a plateau of high speed downstream from the constriction. The area surrounding a flow jet is theoretically constituted by a shear layer which contains vortex-like structures (25). As seen in Fig. 5c, elevated TKE values are detected in the area surrounding the flow jet in the coarctation patient. From fluid mechanics theory, one would expect that turbulent velocity fluctuations are created at the site of jet breakdown and the highest TKE values are measured at this site (Fig. 5c). The interplay between mean and fluctuating velocities in turbulent jet flow is reflected in the evaluation of the mean and turbulent kinetic energy along the sample line in the coarctation patient (Fig. 6). In the systolic time frames, elevated values of MKE are found in the flow jet whereas the highest values of TKE are found distal to the rapid decrease in MKE (see also movie 1). The temporal evolution of TKE (Figs. 6, 8 and Movie 1) in the immediate vicinity of the stenotic anastomosis includes two peaks which reflect the pulsatility of arterial blood flow. In early systole, the acceleration of flow through the constriction creates a jet-like flow that emerges from the constriction. Distal to the jet, the flow contains velocity fluctuations which result in the first temporal TKE peak seen in Figs. 6 and 8. As systole progresses, the length of the jet increases and the flow adjacent to the anastomosis, which was highly disturbed in early systole, becomes more organized and the value of TKE in this area decreases. With the flow deceleration at the end of systole, the jet gets shorter and the second TKE peak appears in the immediate vicinity of the constriction. Over the diastolic part of the cardiac cycle, the low speed flow is not disturbed by turbulent velocity fluctuations and thus low values of TKE are measured.

The theoretical framework underlying IVSD mapping can be used to quantify the statistical dispersion of any intravoxel velocity distribution which has a Fourier transform that is invertible

on a range of k_v-values > 0 (23). This requires that the intravoxel spin velocities can be considered to have a known distribution. By employing the Gaussian distribution, as in this study, a quantitative relationship between IVSD and the PC-MRI signal magnitude is obtained according to Eq. 3. The quantitative aspect of the IVSD method is consequently degraded if the distribution is non-Gaussian. However, the Gaussian distribution is as a result of the central limit theorem commonly used in turbulence theory (25) and has previously been incorporated in several methods relating MR signal loss and turbulence (31). The Gaussian behavior of turbulent velocity fluctuations in blood flow is also supported by energy spectrum analyses of data recorded by hot-film anemometry downstream from a 75 % stenosis in a pig aorta (32). A number of flow phenomena other than turbulence could also cause an intravoxel velocity distribution; elevated IVSD values therefore do not necessarily reflect only turbulent velocity fluctuations. Given that local variations in flow velocities may reflect abnormal hemodynamics, finding elevated IVSD values in these regions is also of potential interest. In shear flow regions characterized by high spatial acceleration, for example, the locally varying velocity field can be expected to affect the PC-MRI signal magnitude. Pipe (33) exploited the fact that this effect is typical for flow near the vessel wall and suggested that this could be used to estimate wall shear stress. For $k_{v_2} = 0$, Eq. 3, which is valid for Gaussian intravoxel velocity distributions (23), is identical with the empirical expression derived by Pipe (33). Based on the theory underlying IVSD mapping, studies focusing on quantifying the statistical dispersion of spin velocities near the vessel wall, rather than in turbulent intraluminal flow, may benefit from exploiting the fact that the IVSD method readily can be adapted to non-Gaussian distributions as well (23). In the present study, high wall shear rate may have contributed to the elevated values of TKE at the outer wall of the ascending aorta in the patient with an aortic valve prosthesis (Fig. 4). Note, however, that elevated TKE values near the vessel wall are not found in other areas in this patient nor in the other subjects. This suggests that the contribution of shear flow to the IVSD values is small as compared to the contribution from turbulence. Further studies are needed to elucidate whether the effect is negligible.

In voxels covering both blood and static tissue, partial volume effects will result in spin velocity distributions which do not reflect the dispersion of blood flow velocities. Furthermore, the distribution may contain more unknown parameters than what can be resolved by two

measurements of $S(k_v)$. Signal ghosting and aliasing may also degrade the results through partial volume effects. Tuning of imaging parameters such as field of view and temporal resolution is thus recommended not only for good image quality but also for retaining the accuracy of the IVSD quantification.

An attractive property of the IVSD method is that it requires no data other than what is commonly acquired with a standard PC-MRI pulse sequence, although the flow encoding scheme must be chosen so that $|k_{v_1}| \neq |k_{v_2}|$. When the VENC for best IVSD sensitivity is not much below the maximum velocity, simple phase-unwrapping schemes may be used to obtain correct velocities from the acquired data. In this work, phase unwrapping incorporating only the temporal domain resulted in the reconstruction of both velocity and IVSD from the single data sets acquired in three of four subjects. The choice of VENC in IVSD measurements can be compared to the choice of VENC in PC-MRI velocity mapping, where matching the estimated peak systolic velocity is most often desired. In IVSD mapping, a 40 % signal loss gives the best sensitivity and the VENC can be chosen accordingly. By improving the SNR or by using a sophisticated phase-unwrapping algorithm, both velocity and IVSD could be obtained from the same data set even in situations where the difference between optimal VENC for velocity and IVSD mapping is broader. The fact that a 40 % signal loss gives the best sensitivity can also be exploited for retrospective assessment of the accuracy of each acquired IVSD value by studying the $S(0)$ and $S(k_v)$ magnitudes. Signal loss that affects both $S(0)$ and $S(k_v)$ does not affect the validity of the IVSD method, as the IVSD is derived from the relative loss of signal magnitude in $S(k_v)$ versus $S(0)$. A low $S(0)$ magnitude will decrease the dynamic range, however, and therefore it is important to maintain a high $S(0)$ magnitude over the imaging volume of interest to reduce the influence of noise. At the edges of the dynamic range the IVSD estimation is degraded by noise; further studies are needed to establish the nature of this effect.

The role of disturbed blood flow in the progression of valve and vessel stenoses has been frequently discussed (6,8,34,35) and highlights the need for a non-invasive tool to study flow disturbances (1,36). In the setting of valvular heart disease, a non-invasive method to quantify blood flow turbulence could improve our understanding of hemodynamic impact and guide surgical correction. Moreover, PC-MRI IVSD mapping may prove to be valuable in investigating

the specific hemodynamic effects of different options for surgical repair. In aortic valve replacement, for example, studies have shown that improved valve hemodynamics are favorably correlated with long term patient survival (37). Fluctuating blood flow has also been proposed as a contributing factor in the pathogenesis of atherosclerosis (3,7,8). In the present study, each scanned patient had a different cardiovascular disease and no general conclusions regarding the flow accompanying each specific condition can be drawn. However, the successful measurement of both the mean and the fluctuating velocity fields in the range of conditions shown here suggests that generalized PC-MRI has the potential to become a valuable tool in investigating the extent, timing and role of turbulent blood flow in the human body, and the interaction between turbulence and progression of cardiovascular disease. For large scale in-vivo studies, scan time is an important issue and 2D IVSD scans may be an option. However, 2D IVSD measurements may be affected by inflow effects (23) and pose a risk of missing the areas of highest turbulence intensity. An alternative option might be to speed up the 3D data acquisition by using parallel imaging and exploiting spatiotemporal correlations (38) in the dynamic data, for example. This could also be used to improve the spatial resolution and thereby allow for IVSD mapping in smaller vessels.

The ability to non-invasively quantify turbulence intensity in 3D is also of great interest for non-medical applications. In complex turbulent engineering flow, PC-MRI velocity mapping has been shown to provide accurate mean velocity data (39). The IVSD method may add a new aspect to the PC-MRI assessment of flow in engineering applications by allowing optimization of components with respect to turbulence (40).

In conclusion, this study supports the hypothesis that non-invasive PC-MRI IVSD mapping is able to detect flow abnormalities in a variety of human cardiovascular conditions. The fact that the highest IVSD values were found in flow situations where turbulent flow is expected implies that IVSD mapping is promising for the detection and quantitative assessment of turbulence. Although the IVSD measurements were not markedly affected by other complex flow phenomena, further investigations are necessary to clarify whether shear flow contribution to the IVSD values is negligible. In combination with velocity mapping, IVSD mapping may allow assessment of regions with flow abnormalities that portend significant hemodynamic impact or

disease progression. This information would address a longstanding gap in our scientific and clinical armamentarium for studying and treating cardiac, valvular and vascular diseases.

REFERENCES

1. Richter Y, Edelman ER. Cardiology Is Flow. Circulation 2006;113:2679-2682.
2. Hinze JO. Turbulence. New York: McGraw-Hill; 1975.
3. Nichols W, O'Rourke M. McDonald's Blood Flow in Arteries. London: Hodder Arnold; 2005.
4. Sallam AM, Hwang NH. Human red blood cell hemolysis in a turbulent shear flow: contribution of Reynolds shear stresses. Biorheology 1984;21:783-797.
5. Stein PD, Sabbah HN. Measured Turbulence and Its Effect on Thrombus Formation. Circulation Research 1974;35:608-614.
6. Becker RC, Eisenberg P, Turpie AG. Pathobiologic features and prevention of thrombotic complications associated with prosthetic heart valves: fundamental principles and the contribution of platelets and thrombin. Am Heart J 2001;141:1025-1037.
7. Malek AM, Alper SL, Izumo S. Hemodynamic shear stress and its role in atherosclerosis. Jama 1999;282:2035-2042.
8. Cheng C, Tempel D, van Haperen R, et al. Atherosclerotic Lesion Size and Vulnerability Are Determined by Patterns of Fluid Shear Stress. Circulation 2006;113:2744-2753.
9. Stein PD, Sabbah HN. Turbulent blood flow in the ascending aorta of humans with normal and diseased aortic valves. Circulation Research 1976;39:58-65.
10. Nygaard H, Paulsen P, Hasenkam J, Pedersen E, Rovsing P. Turbulent stresses downstream of three mechanical aortic valve prostheses in human beings. AATS/WTSA; 1994.
11. Isaaz K, Bruntz JF, Da Costa A, et al. Noninvasive quantitation of blood flow turbulence in patients with aortic valve disease using online digital computer analysis of Doppler velocity data. J Am Soc Echocardiogr 2003;16:965-974.
12. Grigioni M, Daniele C, D'Avenio G, Barbaro V. On the monodimensional approach to the estimation of the highest reynolds shear stress in a turbulent flow. J Biomech 2000;33:701-708.
13. Moran PR. A flow velocity zeugmatographic interlace for NMR imaging in humans. Magn Reson Imaging 1982;1:197-203.
14. Wigström L, Sjöqvist L, Wranne B. Temporally resolved 3D phase-contrast imaging. Magn Reson Med 1996;36:800-803.

15. Gatehouse PD, Keegan J, Crowe LA, et al. Applications of phase-contrast flow and velocity imaging in cardiovascular MRI. Eur Radiol 2005;15:2172-2184.
16. Pennell D, Sechtem U, Higgins C, et al. Clinical indications for cardiovascular magnetic resonance (CMR): Consensus Panel report. Eur Heart J 2004;25:1940-1965.
17. DiCarlo JC, Hargreaves BA, Nayak KS, Hu BS, Pauly JM, Nishimura DG. Variable-density one-shot Fourier velocity encoding. Magn Reson Med 2005;54:645-655.
18. Galea D, Lauzon M, Drangova M. Peak velocity determination using fast Fourier velocity encoding with minimal spatial encoding. Med Phys 2002;29:1719.
19. Nayak K, Hu B, Nishimura D. Rapid quantitation of high-speed flow jets. Magn Reson Med 2003;50:366-372.
20. Oshinski JN, Ku DN, Pettigrew RI. Turbulent fluctuation velocity: the most significant determinant of signal loss in stenotic vessels. Magn Reson Med 1995;33:193-199.
21. Prince M, Schoenberg S, Ward J, Londy F, Wakefield T, Stanley J. Hemodynamically significant atherosclerotic renal artery stenosis: MR angiographic features. Radiology 1997;205:128-136.
22. Wasser M, Westenberg J, van der Hulst V, et al. Hemodynamic significance of renal artery stenosis: digital subtraction angiography versus systolically gated three-dimensional phase-contrast MR angiography. Radiology 1997;202:333-338.
23. Dyverfeldt P, Sigfridsson A, Kvitting JPE, Ebbers T. Quantification of intravoxel velocity standard deviation and turbulence intensity by generalizing phase-contrast MRI. Magn Reson Med 2006;56:850-858.
24. Haacke E, Brown R, Thompson M, Venkatesan R. Magnetic Resonance Imaging: Physical Principles and Sequence Design. New York: John Wiley & Sons; 1999.
25. Mathieu J, Scott J. An Introduction to Turbulent Flow. Cambridge: Cambridge University Press; 2000.
26. Wigström L, Ebbers T, Fyrenius A, et al. Particle trace visualization of intracardiac flow using time-resolved 3D phase contrast MRI. Magn Reson Med 1999;41:793-799.
27. Kvitting JPE, Ebbers T, Wigström L, Engvall J, Olin CL, Bolger AF. Flow patterns in the aortic root and the aorta studied with time-resolved, 3-dimensional, phase-contrast magnetic resonance imaging: implications for aortic valve-sparing surgery. J Thorac Cardiovasc Surg 2004;127:1602-1607.

28. Milano A, Blanzola C, Mecozzi G, et al. Hemodynamic performance of stented and stentless aortic bioprostheses. Ann Thorac Surg 2001;72:33-38.
29. Lim W, Chew Y, Chew T, Low H. Pulsatile flow studies of a porcine bioprosthetic aortic valve in vitro: PIV measurements and shear-induced blood damage. Journal of Biomechanics 2001;34:1417-1427.
30. Kozerke S, Hasenkam JM, Pedersen EM, Boesiger P. Visualization of flow patterns distal to aortic valve prostheses in humans using a fast approach for cine 3D velocity mapping. J Magn Reson Imaging 2001;13:690-698.
31. Kuethe DO, Gao JH. NMR signal loss from turbulence: Models of time dependence compared with data. Phys Rev E 1995;51:3252-3262.
32. Nygaard H, Hasenkam J, Pedersen E, Kim W, Paulsen P. A new perivascular multi-element pulsed Doppler ultrasound system forin vivo studies of velocity fields and turbulent stresses in large vessels. Medical and Biological Engineering and Computing 1994;32:55-62.
33. Pipe JG. A simple measure of flow disorder and wall shear stress in phase contrast MRI. Magn Reson Med 2003;49:543-550.
34. Robicsek F, Thubrikar MJ, Cook JW, Fowler B. The congenitally bicuspid aortic valve: how does it function? Why does it fail? Ann Thorac Surg 2004;77:177-185.
35. Wakhloo AK, Lieber BB, Seong J, et al. Hemodynamics of carotid artery atherosclerotic occlusive disease. J Vasc Interv Radiol 2004;15:S111-121.
36. Yoganathan AP, Chandran KB, Sotiropoulos F. Flow in prosthetic heart valves: state-of-the-art and future directions. Ann Biomed Eng 2005;33:1689-1694.
37. Westaby S, Horton M, Jin XY, et al. Survival advantage of stentless aortic bioprostheses. Ann Thorac Surg 2000;70:785-790; discussion 790-781.
38. Tsao J, Boesiger P, Pruessmann K. kt BLAST and kt SENSE: dynamic MRI with high frame rate exploiting spatiotemporal correlations. Magn Reson Med 2003;50:1031-1042.
39. Elkins CJ, Markl M, Pelc NJ, Eaton JK. 4D magnetic resonance velocimetry for mean velocity measurements in complex turbulent flow. Exp Fluids 2003;34:494-503.
40. Elkins C, Alley M. Magnetic resonance velocimetry: applications of magnetic resonance imaging in the measurement of fluid motion. Exp Fluids 2007;43:823-858.

TABLES

Table 1
Overview of Imaging Parameters

Parameter	Healthy Volunteer [a]	Aortic Insufficiency Patient [a]	Valve Prosthesis Patient [a]	Coarctation Patient Velocity	Coarctation Patient IVSD
VENC [cm s^{-1}]	140	120	200	350	140
Field of View [mm]	278 x 278 x 48	300 x 300 x 75	300 x 300 x 60	272 x 272 x 60	288 x 288 x 54
Matrix Size	96 x 96 x 16	112 x 112 x 24	112 x 112 x 20	80 x 80 x 20	96 x 96 x 18
Echo Time [ms]	3.0	3.0	3.7	3.0	3.0
Repetition Time [ms]	5.2	5.1	6.7	5.4	5.1
SENSE	-	2	2	2	-
Temporal speed-up factor [b]	3	2	2	3	4
Temporal Resolution [ms]	62.4	40.8	53.6	64.8	81.6
Scan Time [c]	7 min 45 sec	10 min 40 sec	10 min 34 sec	6 min 4 sec	10 min 3 sec

[a] In each of these subjects, both the standard deviation of the intravoxel spin velocity distribution (IVSD) and the velocity were reconstructed from the same data set.

[b] Number of sets of four flow encoding segments which were interleaved in order to decrease the scan time.

[c] The scan time is exclusive of the navigator gating efficiency.

FIGURE LEGENDS

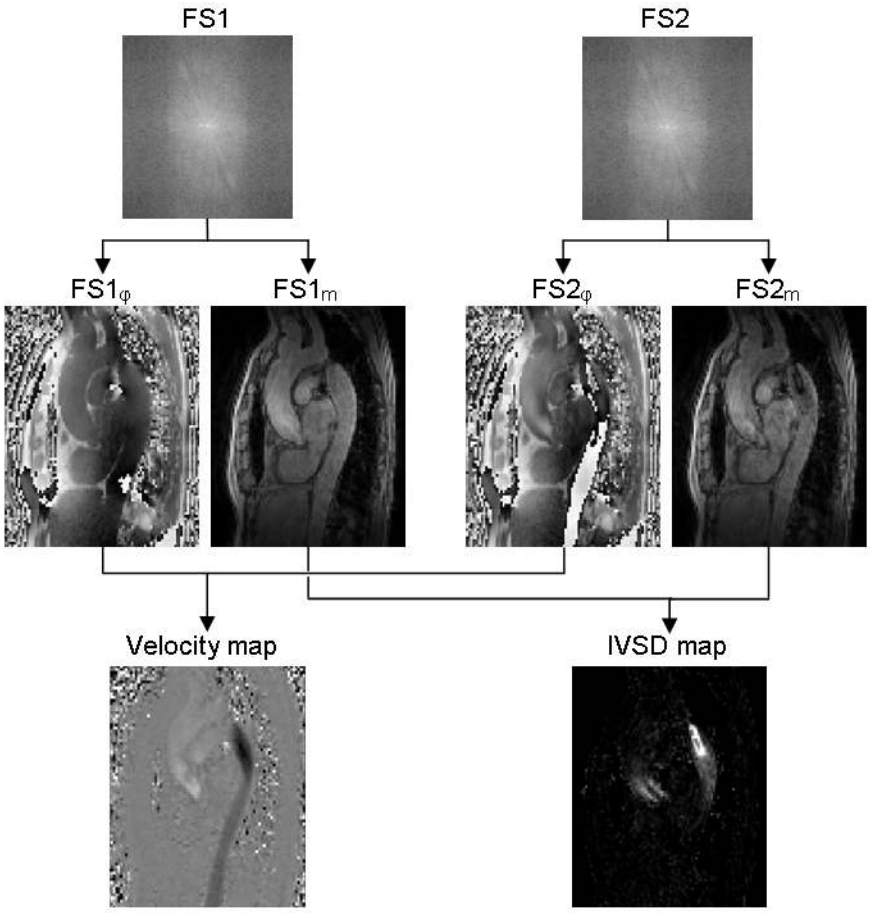

Fig. 1. The fundamental similarities and differences of PC-MRI velocity and IVSD mapping. Two measurements, or flow encoding segments (FS), of different flow sensitivity give rise to two complex-valued PC-MRI signals from which the phase (φ) and the signal magnitude (m) can be obtained. From these data, the velocity can be computed by phase subtraction whereas the IVSD can be obtained from the signal magnitude relationship.

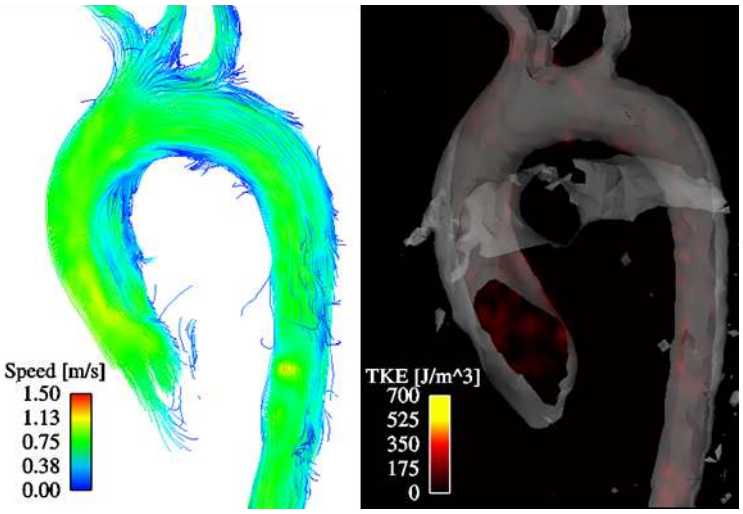

Fig. 2. Aortic blood flow at peak systole in a healthy volunteer visualized by 3D streamlines (a) and a TKE map combined with a semi-transparent iso-surface rendering computed from the PC-MRI data (b).

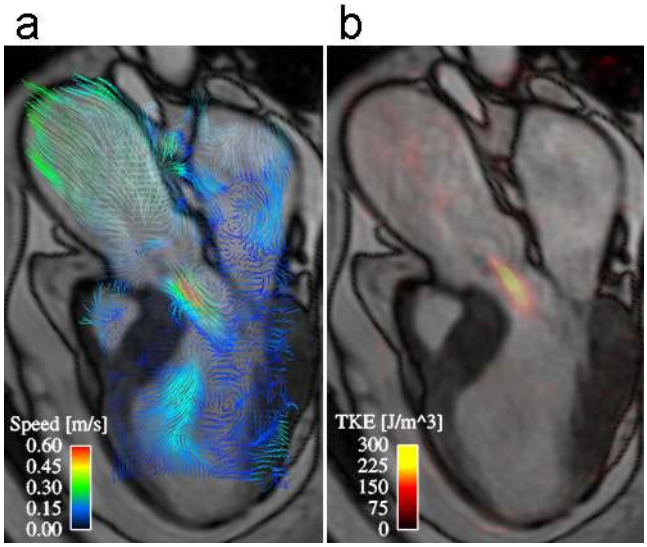

Fig. 3. Visualization of the peak regurgitation flow in a patient with mild aortic insufficiency. 3D streamlines, combined with a semi-transparent b-SSFP three-chamber image (a), reveal a small regurgitation flow into the left ventricular outflow tract. A 2D clip plane, color coded according to scales of TKE, combined with a semi-transparent b-SSFP three-chamber image (b), show elevated values of TKE in the vicinity of the regurgitation flow jet.

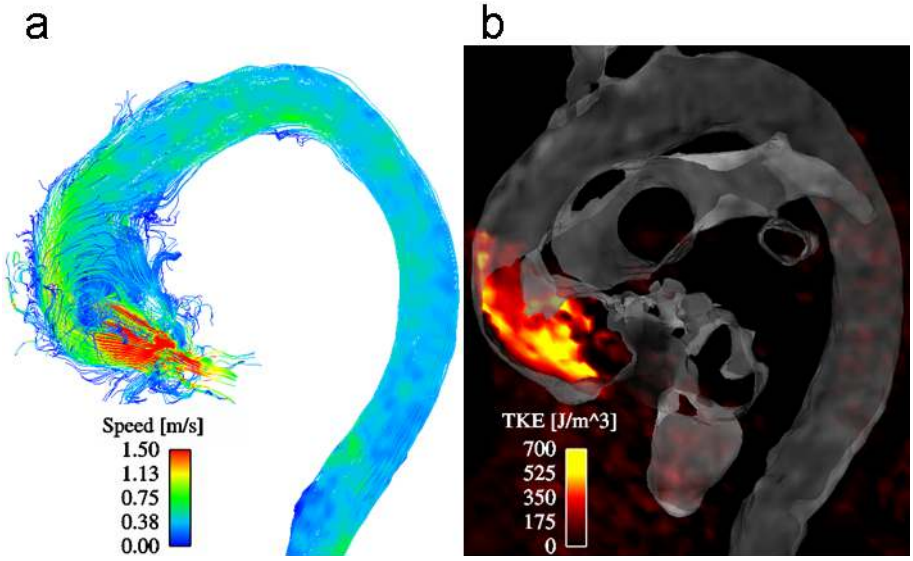

Fig. 4. Aortic blood flow at peak systole in a patient with an aortic valve prosthesis visualized by 3D streamlines (a) and a TKE map showing the turbulence intensity in combination with a semi-transparent iso-surface rendering computed from the PC-MRI data (b).

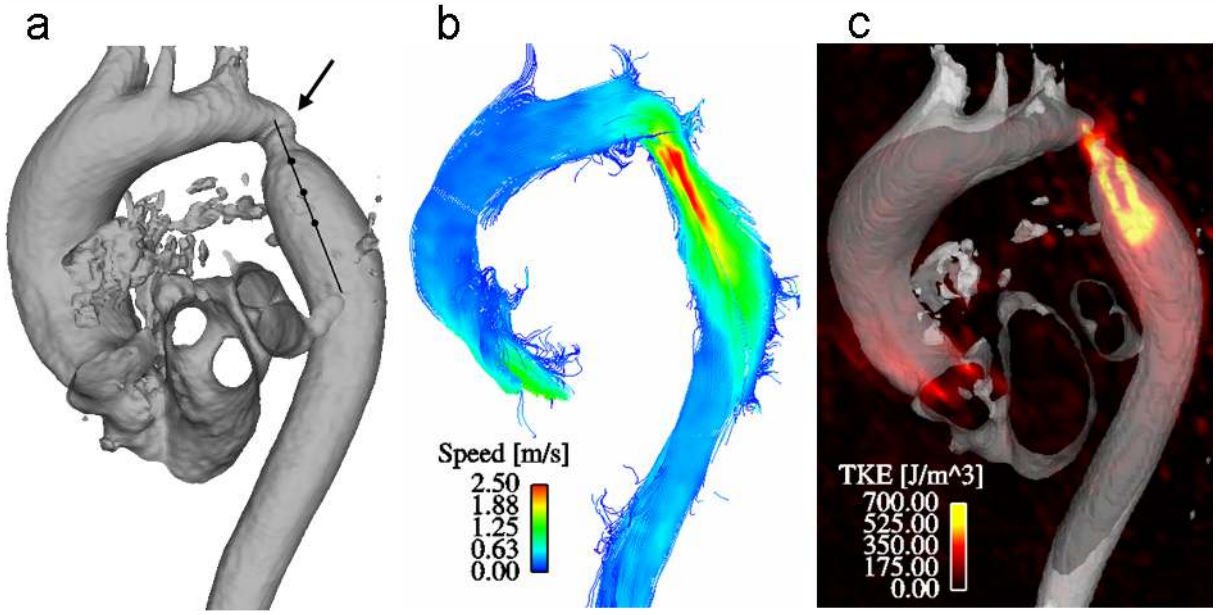

Fig. 5. Visualization of data acquired in a patient with an aortic coarctation. A 3D iso-surface rendering of contrast-enhanced MRA data (a) is shown with a black line, originating from above the anastomotic constriction (arrow) site. This line serves as a sample line for data extraction and the dots show distances relative to the center of the coarctation of approximately one, two and three times the coarctation diameter. Detailed plots of the kinetic energy over time at these locations can be seen in Fig. 8. The peak systolic aortic blood flow is visualized by color-coded 3D streamlines (b) and, in combination with a semi-transparent 3D iso-surface rendering, by a color-coded convex TKE clip surface showing the intensity of the fluctuating velocity field (c). A time-resolved visualization of the TKE can be seen in Movie 1.

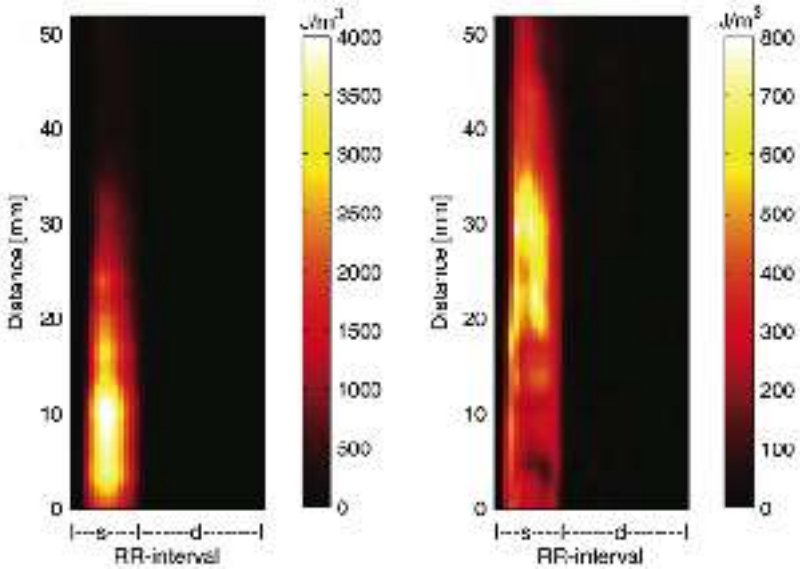

Fig. 6. Temporal evolution of MKE (left) and TKE (right) in the coarctation patient along the sample line shown in Fig. 5. The vertical axis shows the position at the sample line and the horizontal axis shows the timing of the cardiac cycle (RR-interval) where the approximate durations of systole (s) and diastole (d) are indicated. The center of the stenosis is located at approximately 3 mm from the origin of the sample line.

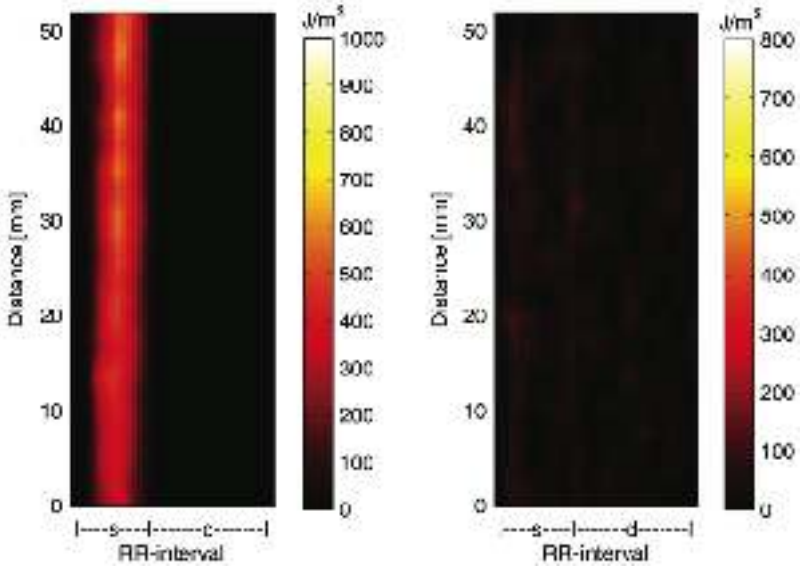

Fig. 7. Temporal evolution of MKE (left) and TKE (right) in the healthy volunteer along a sample line corresponding to the one in the coarctation patient (Fig. 5). The vertical axis shows the position at the sample line and the horizontal axis shows the timing of the cardiac cycle (RR-interval) where the approximate durations of systole (s) and diastole (d) are indicated. Note the different MKE color scales in Figs. 6 and 7.

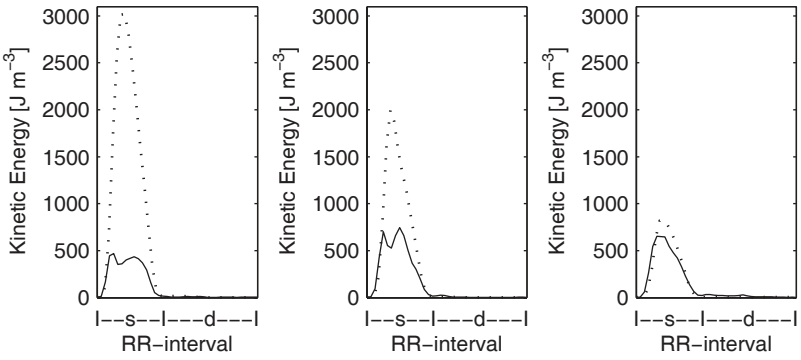

Fig. 8. Plots of TKE (solid line) and MKE (dotted line) in the coarctation patient over the cardiac cycle (RR-interval) at distances of one (left), two (middle) and three (right) coarctation diameters downstream from the center of the constriction according to the dots drawn in Fig. 5. Below the plots, the approximate durations of systole (s) and diastole (d) are indicated. Note that, as the distance from the stenosis increases, the peak MKE value decreases while the TKE reaches its highest values at the two most distant locations.

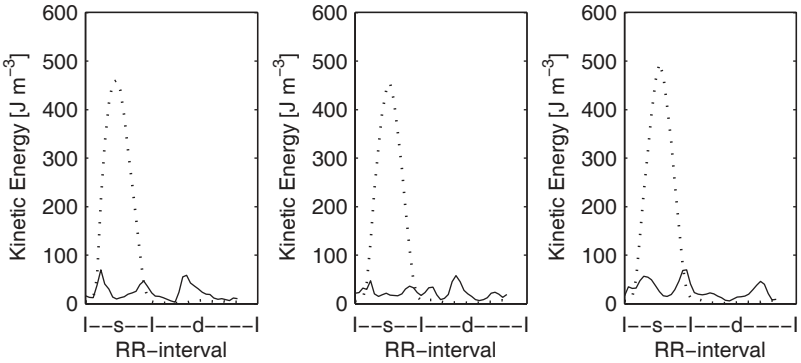

Fig. 9. Plots of TKE (solid line) and MKE (dotted line) in the healthy volunteer over the cardiac cycle (RR-interval) at three different locations corresponding to the ones in Fig. 8. Below the plots, the approximate durations of systole (s) and diastole (d) are indicated. Note that the peak MKE value is approximately the same at all locations and that the TKE is low compared to the values observed in the coarctation patient (Fig. 8). Note the different KE scales between Figs. 8 and 9.

MOVIE LEGENDS (Supplementary Material)

Movie 1. Time-resolved visualization of TKE in the aortic coarctation patient. A convex clip surface, color coded according to TKE, shows the intensity of the turbulent velocity fluctuations. A 3D iso-surface rendering of contrast enhanced MRA data outlines the geometry. Sparse 3D streamlines, emitted from the center of the coarctation, outline the instantaneous mean velocities near the coarctation at each time frame. Plots on the left hand side demonstrate the temporal evolution of TKE (top), MKE (middle) and speed (bottom) downstream from the coarctation at the location indicated by the white dot. The highest values of TKE can be observed downstream from the coarctation in the areas surrounding the flow jet. At peak systole (Time = 0.206), the flow jet extends through the sample point and causes a decrease in TKE which can be seen both in the TKE map and the plot. Elevated values of TKE can also be observed in the aortic root downstream from the abnormal subaortic membrane which was present in this patient. Note that, at the center of the constriction, the TKE surface blocks the view of the iso-surface.